ROYAL SOCIETY OF CHEMISTRY

PAPER

Check for updates

Phase-pure BiFeO₃ produced by reaction flash-sintering of Bi₂O₃ and Fe₂O₃†

Eva Gil-González,[a] Antonio Perejón, [ID][ab] Pedro E. Sánchez-Jiménez,[a] María J. Sayagués,[a] Rishi Raj[c] and Luis A. Pérez-Maqueda [ID] *[a]

Mixed powders of Bi₂O₃ and Fe₂O₃ are shown to yield single-phase, dense nanostructured polycrystals of BiFeO₃ in reaction flash sintering experiments, carried out by applying a field of 50 V cm⁻¹ and with the current limit set to 35 mA mm⁻². The furnace was heated at a constant rate with the reaction sintering taking place abruptly upon reaching 625 °C. Remarkably, an intermediate bismuth-rich phase of the oxide that forms just before reaching the flash temperature transforms, and at the same time sinters, into single-phase BiFeO₃ within a few seconds after the onset of the flash. The BiFeO₃ so produced is electrically insulating, a property that is critical to its applications. This one-step synthesis of single-phase polycrystals of complex oxides from their basic constituents, by reaction flash sintering, is a significant development in the processing of complex oxides, which are normally difficult to sinter by conventional methods.

1. Introduction

Looking for new methods of synthesis has always been a matter of research in materials chemistry.[1] The current trend is not only to discover fast, energy-efficient and environmentally friendly approaches, but also to induce chemical reactions that are far from equilibrium by various kinds of excitations. For instance, in mechanochemistry, mechanical energy can produce chemical reactions.[2,3] Microwave radiation is employed in the synthesis of organic and inorganic compounds.[4–7] Lasers have been applied to synthesize materials with control at the nanometric scale.[8,9] Sonochemical-based methods use ultrasound irradiation to produce liquid phase reactions, induced by cavitation.[10]

Electric field assisted-methods have shown that electric current enhances the kinetics of inter-diffusion processes in solid-state reactions.[11] In Spark Plasma Sintering (SPS), pulsed, high DC currents have been used for synthesis.[11–14] However, the highly reducing conditions in SPS can degrade the properties of the resulting materials. For example, BiFeO₃ sintered by SPS suffers from high leakage current.[15] The application of modest electric fields (few tens of V cm⁻¹) and small DC currents (tens of mA mm⁻²) can produce a sharp increase in conductivity and electroluminescence, which is accompanied by sudden sintering at low furnace temperatures.[16,17] This approach, called "Flash Sintering", has been applied to the densification of a number of different materials.[18–31]

The aim of the present work is to explore if chemical reactions and sintering can be merged into a single step in flash experiments. We are able to show that single phase, nearly dense, polycrystals of BiFeO₃ can be synthesized from powders of Bi₂O₃ and Fe₂O₃ in just a few seconds; we call it reaction flash sintering (RFS).

BiFeO₃ is a multiferroic material at room temperature, with potential applications in data storage, magnetoelectric sensors and even photocatalytic applications.[32–38] Nevertheless, the difficulties in obtaining pure phase, highly insulating materials is hindering its application. Thus, for example, high performance epitaxially grown BiFeO₃ thin films can be prepared by pulsed laser deposition only from phase-pure ceramic targets.[39] In previous work we have shown that high quality BiFeO₃ pellets could be obtained by flash sintering of pure BiFeO₃ nanoparticles.[40] In the present work, we show that similar results can be obtained in just one step from simple oxides, Fe₂O₃ and Bi₂O₃, where the reaction and sintering occur concurrently. The results presented here open the door to using flash to produce single-phase compounds of complex oxides in a single step from basic starting materials, which is normally not possible (or very difficult) by conventional methods.

[a]Instituto de Ciencia de Materiales de Sevilla (C.S.I.C.-Univ. Sevilla), C. Américo Vespucio 49, Sevilla 41092, Spain. E-mail: maqueda@cica.es

[b]Departamento de Química Inorgánica, Facultad de Química, Universidad de Sevilla, Sevilla 41071, Spain

[c]Materials Science and Engineering Program, Department of Mechanical Engineering, University of Colorado at Boulder, Boulder, CO 80309-0427, USA

† Electronic supplementary information (ESI) available. See DOI: 10.1039/c7ta09239c

2. Experimental

2.1 Sample preparation

Stoichiometric mixtures of Bi₂O₃ (Sigma-Aldrich 223891-500G, 10 μm, 99.9% purity) and Fe₂O₃ (Sigma-Aldrich 310050-500G, <5 μm, ≥99% purity) were ball-milled for 15 minutes to obtain a homogenous mixture of the starting oxides. Approximately
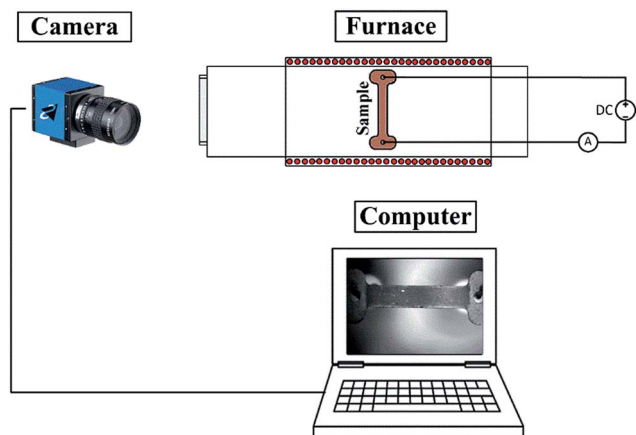
Fig. 1 Scheme of the experimental setup used for the flash experiments.

800 mg of the powders were pressed into dog-bone shaped specimens by applying a uniaxial pressure of 250 MPa. Platinum paste was applied into the holes of the handles of the green-body samples, in order to improve the electrical contact with the platinum wires which served as electrodes as well as "hangers" for placing the specimens in the furnace. These wires were connected to an EA-PS 8720-15 DC power supply of 3000 W (EA Elektro Automatik, Helmholtzstraße, Germany). Current and voltage measurements were taken by means of a two channel

Keithley 2110 5 1/2 digital multimeter (Keithley Instruments, Cleveland, USA). The shrinkage of the samples was monitored by using a 1/3 inch Sony CCD sensor camera (Imaging Source DMK 23U445). A scheme of the experimental setup is presented in Fig. 1.

The experiments were performed at a constant heating rate of 10 °C min^{-1} in an air flow of 100 cm^3 min^{-1}. Electric fields ranging from 25 to 100 V cm^{-1} were applied until the reactive flash event took place. This event was signalled by a non-linear rise of the conductivity. When the current reached a prescribed limit, the power supply was switched from voltage to current control. The current intensity limit was set in the range of 20–50 mA mm^{-2}. In every experiment, the flash state was maintained for approximately 60 seconds before the power supply was switched off and the furnace was allowed to cool down. Images of the specimen were acquired with the camera at a rate of one per second. A movie of the flash experiment at an applied voltage of 50 V cm^{-1} and a current intensity limit of 35 mA mm^{-2} is included in the ESI;† it shows that sample shrinkage is accompanied by electroluminescence.

2.2 Sample characterization

XRD data were collected on a Rigaku Miniflex diffractometer working at 45 kV and 40 mA. Additionally, the pattern for Rietveld refinement was collected on a PANalytical X'Pert PRO diffractometer, working at 45 kV and 40 mA, using CuK$_\alpha$ radiation and equipped with an X'Celerator detector and a graphite
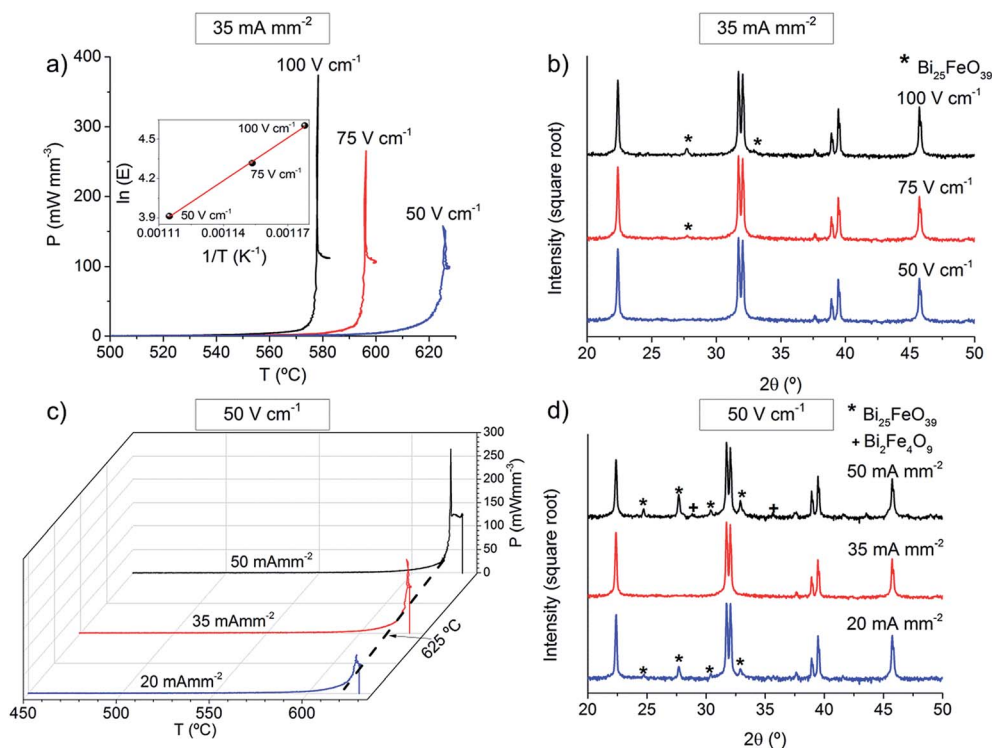

Fig. 2 Power dissipation profiles (a) and X-ray diffraction patterns (b) of the resulting pellets obtained under different electric fields and a current limit of 35 mA mm^{-2}, and power dissipation profiles for an electric field of 50 V cm^{-1} and different current limits (c) and their corresponding X-ray diffraction patterns (d). The intensity of the X-ray diffraction patterns is represented in square root in order to make the secondary phases more noticeable.

diffracted beam monochromator. FullProf software was used for the Rietveld refinement.[41]

Differential scanning calorimetry experiments were performed using a simultaneous TG/DSC instrument (Q600 SDT, TA Instruments, Crawley, UK) in the temperature range from 250 °C to 850 °C. The samples were placed in open alumina pans and the DSC curves were recorded on heating and cooling at 10 °C min^{-1} under an air flow of 100 cm^3 min^{-1}.

SEM micrographs were collected using a Hitachi S-4800 SEM-FEG, equipped with an energy dispersive X-ray spectrometer (EDX), Quantax Bruker. The field-emission gun was operated at 2 kV in order to obtain the micrographs, while for EDX analysis, it was operated at 20 kV. The samples were Au sputter-coated at room temperature in an Emitech K550 Sputter Telstar.

The reaction mechanism was characterized by using a high resolution TEM with a field emission gun (FEG-HRTEM) from FEI Company, USA, (Model TECNAI G2 F30 S-twin), with a Fischione Instruments (USA) high angle annular dark-field detector (HAADF, 0.16 nm point resolution) to work in STEM mode, and one INBCA ZX-max 80 silicon drift detector for EDS analysis. The experiments were performed at 300 kV with a resolution of 0.2 nm. The samples were prepared by dispersing the powders in isopropanol for 1 hour, picking up a drop of the diluted supernatant and the subsequent deposition in a glass sample holder. Immediately, a carbon coated grid was smoothly rubbed onto the deposited drops, and finally the grids were dried slowly at room temperature for the solvent to evaporate. The analysis of high resolution micrographs and the fast Fourier transform for phase interpretation were performed with Digital Micrograph software (Gatan Inc., USA) and the Java version of JEM Software. Additionally, the microstructural characterization was carried out using a STEM TALOS F200S, working at 200 kV and 5 nA. The BiFeO$_3$ foil was prepared by means of a Gatan 691 PIPS.

The impedance measurements were collected using a PMS 1735 Newtons4th Ltd Impedance Analyser (UK), over the frequency range from 100 Hz to 1 MHz, at an ac measuring voltage of 0.1 V and in a temperature range from 300 °C to 380 °C. Measurements were carried out taking into account the blank capacitance of the conductivity jig and the overall pellet geometry, whose opposite faces were previously Au sputter-coated using an Emitech K550 Sputter Telstar.

3. Results

The present experiments were carried out by applying an electric field to the specimen and heating the furnace at a constant rate. The onset of flash occurs when the specimen reaches a specific temperature (which depends on the electric field). The abrupt rise in the conductivity is a signature event of the flash onset. As the current rises, it is limited by switching the power supply from voltage to current control. The power density, P, dissipated in the specimen is given by $P = JE$, where J is the current density and E is the electric field. P reaches a peak when the power supply is switched, its value at the peak being given by the product of the applied field and the current limit. Experimental graphs of P, as a function of temperature, for

various fields and current density limits are shown in Fig. 2. Fig. 2a shows the curves for different fields, 50 V cm^{-1} to 100 V cm^{-1}, at the same current limit, 35 mA mm^{-2} (flash did not occur at a lower field of 25 V cm^{-1}). A linear Arrhenius type of relationship between the applied voltage and the flash onset temperature is expected,[42] which is confirmed by the inset in Fig. 2a. Fig. 2c illustrates the effect of current intensity for a constant applied field of 50 V cm^{-1}.
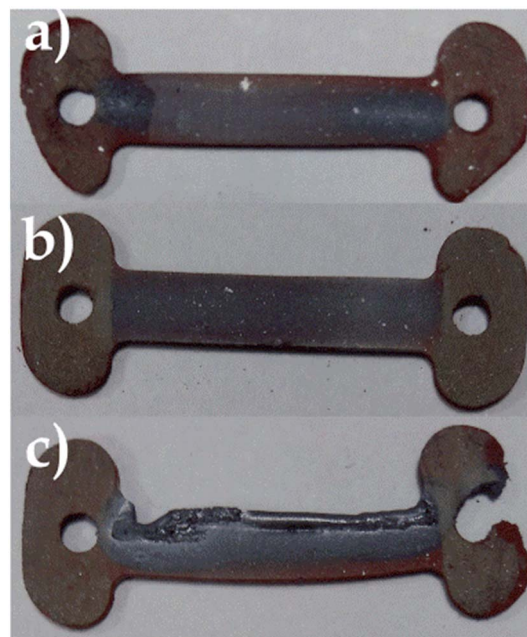

Fig. 3 Photographs of the specimens synthesized by reaction flash sintering at (a) 100 V cm^{-1}, 35 mA mm^{-2}, (b) 50 V cm^{-1}, 35 mA mm^{-2} and (c) 50 V cm^{-1}, 50 mA mm^{-2}.
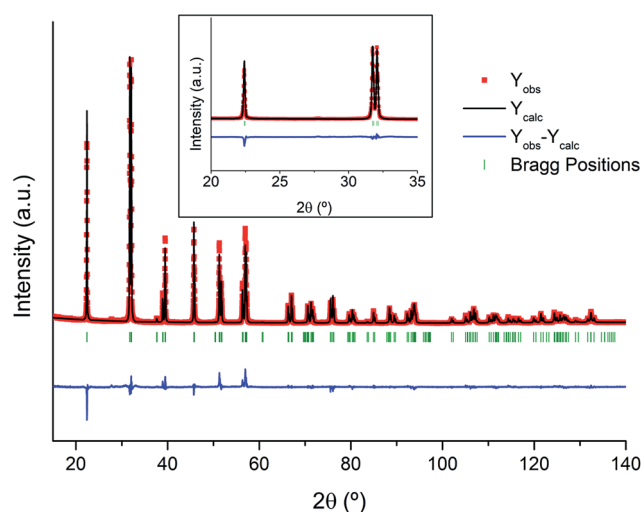

Fig. 4 XRD pattern of BiFeO$_3$ obtained by reaction flash sintering at 50 V cm^{-1} and a current limit of 35 mA mm^{-2} (dots). The solid line corresponds to the fit from the Rietveld refinement. Bragg reflections for the $R3c$ space group are indicated by sticks. The inset shows an expanded section of the diffractogram in the 2θ region from 20° to 35°.

5358 | *J. Mater. Chem. A*, 2018, **6**, 5356–5366

This journal is © The Royal Society of Chemistry 2018

Table 1 Structural parameters and confidence factors obtained from the Rietveld refinement of the XRD pattern of $BiFeO_3$ synthesized by reaction flash sintering at 50 V cm^{-1} and a current limit of 35 mA mm^{-2}

$BiFeO_3$

Cell parameters

R3c

a (Å)	b (Å)	c (Å)
5.5795(2)	5.5795(2)	13.8756(1)

Volume (Å^3)

373.950(3)

Atomic positions

Bi	Fe	O (1)
0.00	0.00	0.43094(2)
0.00	0.00	0.01363(3)
0.00	0.22074(4)	0.95496(5)

Confidence factors

R_{Bragg}	R_{exp}	R_{wp}	χ^2
7.2	4.9	9.3	3.6

Both the applied voltage and the current limit influence the phase constitution of the resulting materials. This is illustrated in the X-ray diffraction patterns in Fig. 2b and d (the intensity of the diffractograms has been depicted in square root so that the secondary phases are more noticeable). Note that a phase-pure material is obtained within a narrow range of experimental conditions, corresponding to an applied voltage of 50 V cm^{-1} and a current intensity limit of 35 mA mm^{-2}. Other experimental conditions produced mixtures with secondary phases. Pictures of samples flashed under different conditions are included in Fig. 3. It is clear that only the said optimum conditions resulted in a homogeneously sintered sample without any distortion of the current flow. In other cases the current became localized causing non-uniform sintering.

Rietveld refinement of the X-ray pattern for the "optimum" $BiFeO_3$ sample, described above, was carried out in order to obtain reliable information on the phase-purity and crystal structure. These results, given in Fig. 4, show that the experimental X-ray profile fits well the calculated pattern, using an *R3c* space group, with good confidence factors (Table 1). Moreover, there is no evidence of any additional peak (the inset of Fig. 4 represents an expanded region from 20° to 35°, where the peaks of the typical secondary phases $Bi_{25}FeO_{39}$ and $Bi_2Fe_4O_9$ would have been noticeable), confirming that we succeeded in synthesizing a phase-pure $BiFeO_3$ perovskite.

Complex impedance spectroscopy (IS) is sensitive to the stoichiometry, phases, vacancies, changes in the oxidation state and microstructure.[43] IS has been shown to be particularly
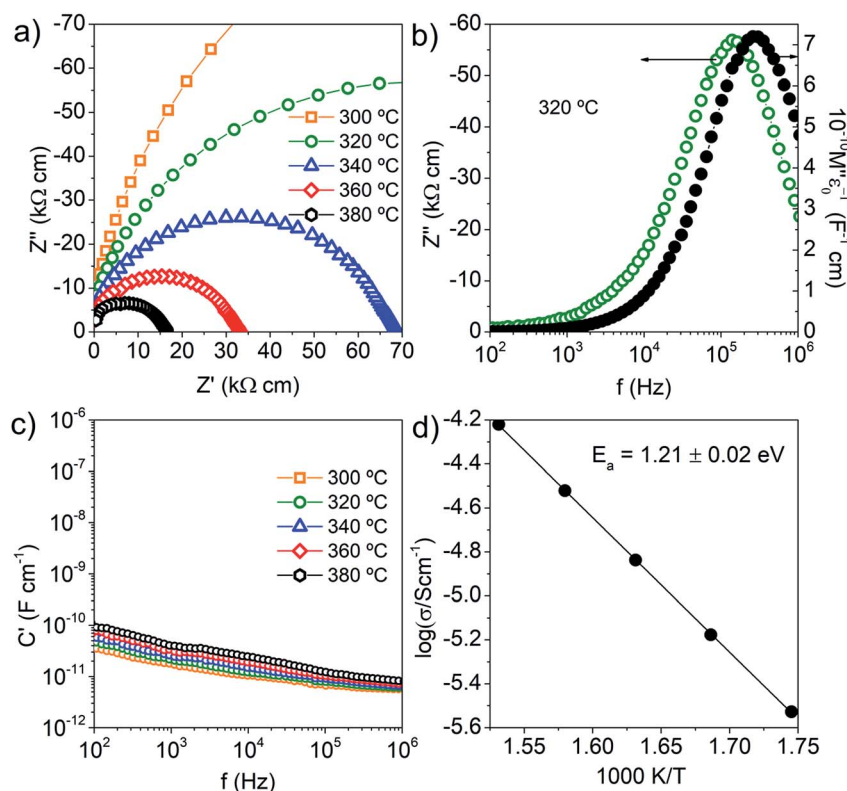
Fig. 5 (a) Impedance complex-plane plots, (b) Z''/M'' spectroscopic plots at 320 °C, (c) C' *versus* frequency and (d) bulk Arrhenius plot of $BiFeO_3$ prepared by reaction flash sintering at 50 V cm^{-1} and a current limit of 35 mA mm^{-2}.
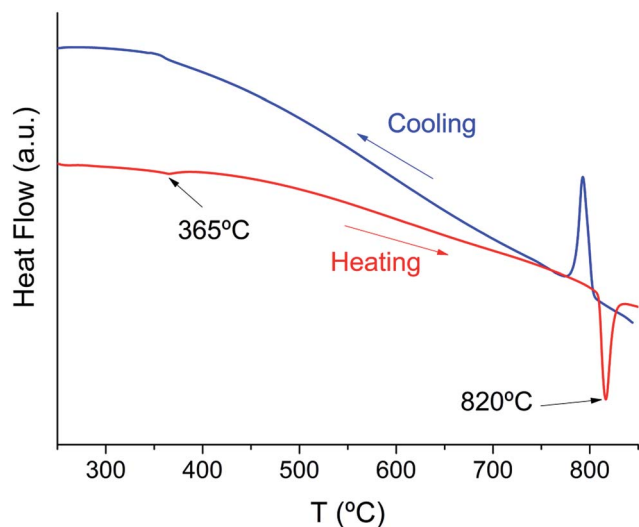
This journal is © The Royal Society of Chemistry 2018

J. Mater. Chem. A, 2018, **6**, 5356–5366 | **5359**

Fig. 6 DSC trace registered at 10 °C min^{-1} on heating and cooling for BiFeO$_3$ prepared by reaction flash sintering at 50 V cm^{-1} and a current limit of 35 mA mm^{-2}.

sensitive to determine the quality of BiFeO$_3$ samples in terms of their stoichiometry and the presence of secondary phases, or oxygen vacancies.[15,40] IS results of the BiFeO$_3$ sample prepared under optimum conditions, 50 V cm^{-1} and 35 mA mm^{-2}, are shown in Fig. 5. The sample is highly insulating at room temperature with only a modest level of semiconductivity above 250 °C. Fig. 5a shows the impedance complex-plane plots collected from 300 °C to 380 °C. They are composed of single, slightly distorted semicircular arcs, which suggests that the material is electrically homogeneous. Fig. 5b shows the impedance, Z'', and modulus, M'', represented as a function of frequency at 320 °C. It can be observed that both signals are single peaks with almost coincident frequency maxima, which further confirms that the sample is electrically homogeneous. Fig. 5c shows the capacitance values at the different temperatures, which remain approximately constant in the entire frequency range. A small plateau is observed at high frequencies, with a value of ~5 pF, followed by a small increment at low frequencies. The bulk conductivity data, in Arrhenius format, are represented in Fig. 5d. Extrapolating from the Arrhenius
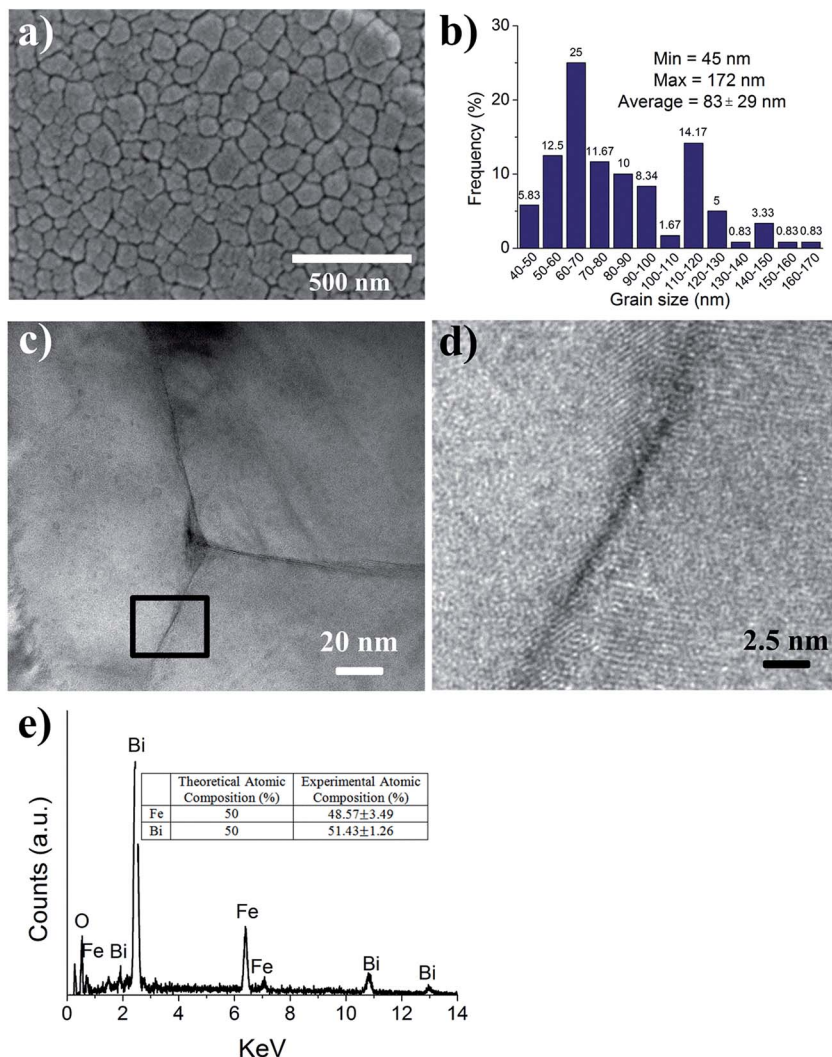

Fig. 7 (a) SEM micrograph, (b) grain size distribution histogram, (c) HRTEM image of a triple junction, (d) grain boundary detail of the selected area marked in (c) and (e) EDX spectrum and elemental atomic composition of BiFeO$_3$ obtained by reaction flash sintering at 50 V cm^{-1} and 35 mA mm^{-2}.

5360 | *J. Mater. Chem. A*, 2018, **6**, 5356–5366

This journal is © The Royal Society of Chemistry 2018

plot, the resistivity value at room temperature is $\sim 2 \times 10^{15}\ \Omega$ cm, which proves that a highly resistive material has been obtained. Additionally, the activation energy, 1.21 eV, is in good agreement with the values reported for high quality samples.[15,33] Therefore, IS confirms that the material obtained by RFS is highly insulating at room temperature and is electrically homogeneous.

Differential scanning calorimetry (DSC) is a useful technique to study the quality of $BiFeO_3$, since thermal effects and phase transition temperatures depend on the presence of impurities.[44–47] Fig. 6 presents a DSC trace registered on heating and cooling between 250 °C and 850 °C for the $BiFeO_3$ sample obtained under optimum conditions. Two endothermic peaks are obtained in this temperature range; at 365 °C a weak transition is observed that corresponds to the antiferromagnetic–paramagnetic transition (T_N), while at 820 °C the sharp peak indicates the ferroelectric–paraelectric transition (T_C), also known as the α–β transition. On cooling, a hysteresis is obtained only for T_C, because the T_N is a second order phase transition. These results are in good agreement with high quality samples of $BiFeO_3$.[45–47]

The final density of the specimen obtained under the optimum flash reaction conditions was 87% of the theoretical density for $BiFeO_3$, as measured by the Archimedes method. The microstructure of the $BiFeO_3$ sample was characterised by SEM, TEM and EDX (Fig. 7). The chemical composition was homogeneous within the entire sample as deduced by using the representative experimental elemental atomic composition spectrum obtained by EDX (Fig. 7e), which shows that the composition of the sample is in close agreement with the theoretically expected values. The microstructure of the sample corresponds to a well-sintered nanostructured material (Fig. 7a). The grain size distribution histogram (Fig. 7b) was calculated by measuring the longest diameters of the grains in the scanning electron micrograph presented in Fig. 7a. A fairly uniform distribution with an average grain size of 83 ± 29 nm was obtained. HRTEM images of a triple junction (Fig. 7c) and an enlargement of the marked grain boundary, (Fig. 7d) show crystalline grains with sharp interfaces between these crystalline grains, without any evidence of amorphous phases.

In contrast, SEM micrographs (Fig. S1 and S2†) corresponding to the samples shown in Fig. 3a and c flashed under non-optimum conditions, show a highly heterogeneous microstructure with melted areas, large pores and even unsintered parts.

For the sake of comparison, a $BiFeO_3$ sample was synthesized using the conventional solid-state reaction procedure. Thus, Bi_2O_3 and Fe_2O_3 powders were mixed stoichiometrically in an agate mortar using ethanol, and the powder was heated at 800 °C for 30 min. Then, the powder was milled again in the mortar and a pellet was prepared, which was subsequently heated at 850 °C for 15 minutes. The density of the pellet was 81%. Fig. S3† shows the X-ray diffraction pattern of the sample, in which the diffraction peaks corresponding to the secondary phases $Bi_{25}FeO_{39}$ and $Bi_2Fe_4O_9$ are evident in the 2θ range of 22–32°. Fig. S4† presents the SEM micrograph of a cross section of the pellet. A heterogeneous microstructure is observed, with

a grain size in the range of 2–0.5 μm, much larger than the grains of the sample flashed under optimum conditions. Moreover, the lower density, as compared to that of the flashed sample, is confirmed by the presence of pores with sizes up to 0.5 μm.

4. Discussion

In this study, we have investigated reaction flash sintering (RFS) where simple oxides (Bi_2O_3 and Fe_2O_3) can react and sinter at the same time to produce a single phase of a complex oxide, $BiFeO_3$.

The preparation of $BiFeO_3$ as a pure highly-insulating compound, by conventional methods, is extremely challenging,[44,48–50] principally because $BiFeO_3$ is a metastable phase. The Gibbs energy differences between $BiFeO_3$ and the secondary phases $Bi_{25}FeO_{39}$ and $Bi_2Fe_4O_9$ are so small that $BiFeO_3$ decomposes easily into these two compounds.[47,51,52] Therefore, $BiFeO_3$ is unstable at temperatures needed to induce a solid–solid reaction between Bi_2O_3 and Fe_2O_3. Furthermore, it has been shown that above the α–β transition $BiFeO_3$ decomposes according to the Avrami−Erofeev nucleation and growth model.[45] Poor electrical properties such as high leakage current, dielectric loss and spontaneous polarization are attributed to the presence of such secondary phases.[53–56]
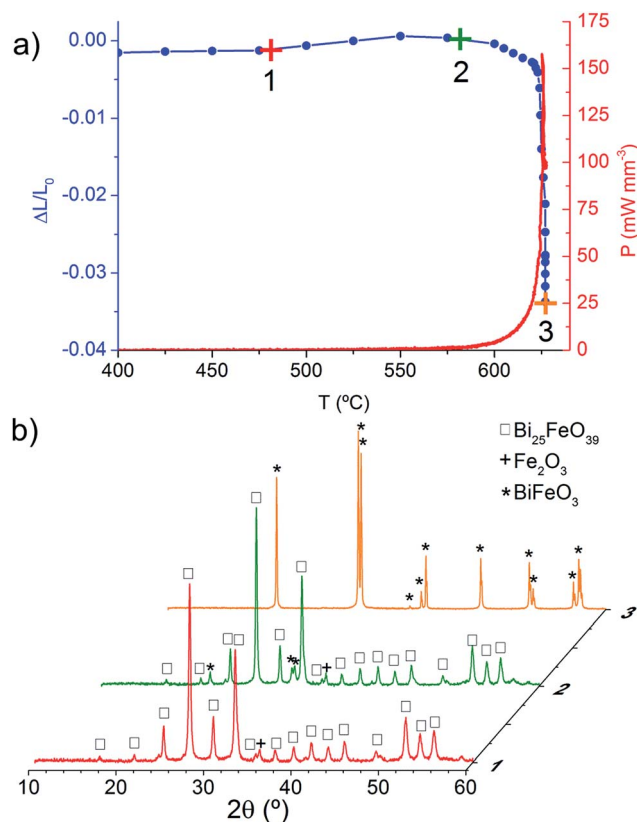

Fig. 8 (a) Linear shrinkage curve, $\Delta L/L_0$, and power dissipation, P, as a function of furnace temperature and (b) *ex situ* XRD patterns of the sample at points #1, #2 and #3 marked in (a).

This journal is © The Royal Society of Chemistry 2018

J. Mater. Chem. A, 2018, **6**, 5356–5366 | **5361**

In this work, we have demonstrated that it is possible to produce phase-pure specimens of $BiFeO_3$ by reaction flash sintering that are electrically homogeneous and highly insulating, within a narrow window of the electric field and current density. It is intriguing

(i) why the formation of secondary phases is prevented in RFS,

(ii) why the reaction between the constituent oxides occurs so quickly, and

(iii) why the sintering and reaction can occur at the same time at an equal pace.

It is to be expected that Joule heating which induces a rise in the specimen temperature[57,58] plays a role, for example the higher temperature can accelerate sintering.[59] Nevertheless, whether or not Joule heating alone can explain sintering in mere seconds remains controversial.[60] Other effects, obtained from *in situ* experiments at synchrotrons have been reported, for example (i) anisotropic lattice expansion which has been attributed to defect generation,[61] (ii) emergence of new phases during flash[62] and (iii) significant differences between the measured optical emission spectrum and black body radiation anticipated from the measurement of the specimen temperature using the platinum standard.[57] There are also reports of *in situ* TEM studies where even a non-contacting electric field produces enhancement in the shrinkage of the agglomerates[63]

or modification of the grain-boundary mobility.[64] It has been reported that electric current produces an increase in the diffusion coefficient in diffusion couples.[65–67]

The present work shows that iron and bismuth oxides can be reacted during flash to produce single phase $BiFeO_3$. Thus, the question arises whether the electric field modifies the reaction mechanism, in comparison to the solid-state reactions that have been studied in the past. Therefore, the flash experiment was interrupted at different stages and the specimens were examined *ex situ* by X-ray diffraction, high resolution TEM, and SEM-EDX. Fig. 8a shows the linear shrinkage and power dissipation, P, as a function of temperature (the experiment was done at a constant heating rate of 10 °C, 50 V cm^{-1} and 35 mA mm^{-2}). The specimens were extracted at the three points as marked in the figure.

X-ray diffraction data from the above samples are shown in Fig. 8b. Point #1 corresponds to a furnace temperature of 480 °C, which is much below the temperature of the flash event. At this point diffraction peaks corresponding to residual Fe_2O_3 and $Bi_{25}FeO_{39}$ produced by an incipient reaction of the iron and bismuth oxides, are observed. Chemical mappings in the SEM micrographs of Fig. 9 show a heterogeneous material where bismuth enriched areas are predominant on the surface, supporting the formation of $Bi_{25}FeO_{39}$. These results agree with previous studies of the diffusion process according to the
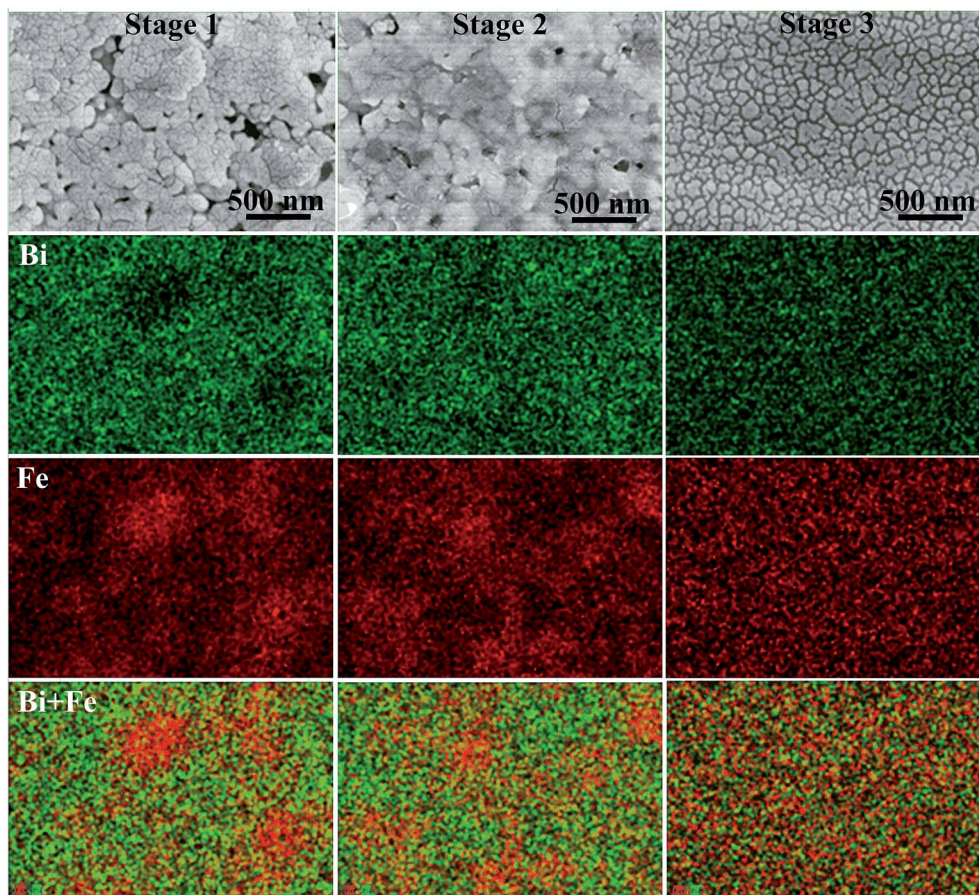

Fig. 9   SEM micrographs (backscattered electrons) and chemical mappings by SEM-EDX taken at points #1, #2 and #3 marked in Fig. 8a. Bi = green and Fe = red.

Kirkendall effect, where it has been concluded that Bi^{3+} ions diffuse into Fe_2O_3 particles.[48] It is of note that $Bi_{25}FeO_{39}$ is often an intermediate phase before the formation of $BiFeO_3$ in different methods of synthesis, including solid-state reaction,[18] hydrothermal precipitation[68] and mechanosynthesis.[19]

Point #2 in Fig. 8a corresponds to a furnace temperature of 580 °C, just before the onset of the flash. This sample has a composition similar to that at point #1; $Bi_{25}FeO_{39}$ and some Fe_2O_3 are the main phases, although very small peaks of $BiFeO_3$ start to emerge (Fig. 8b). Chemical mappings shown in Fig. 9 show a more homogeneous material than that at point #1, but still with a bismuth enriched surface. The Bi and Fe atomic percentages as obtained by EDX analysis, marked on the

surfaces of the four nanograins in Fig. 10c, also corroborate an enriched bismuth surface. TEM analysis shows the presence of $Bi_{25}FeO_{39}$ particles on the surface of the material. Fig. 10a displays a SAED pattern belonging to $Bi_{25}FeO_{39}$, which is oriented along the [1 0 2] zone axis of the cubic structure (I_{23} space group). Another crystal of about 150 nm can be observed in the high resolution micrograph in Fig. 10b, with an interplanar spacing of 0.72 nm corresponding to the (110) plane. Small nanoparticles of $Bi_{25}FeO_{39}$, 5–10 nm, are seen deposited on the edges of the larger particles in this figure.

A dramatic change in the X-ray diffraction pattern is evident in the sample extracted at Point #3 (Fig. 8a) immediately after the flash event which takes place 625 °C and lasts just a few
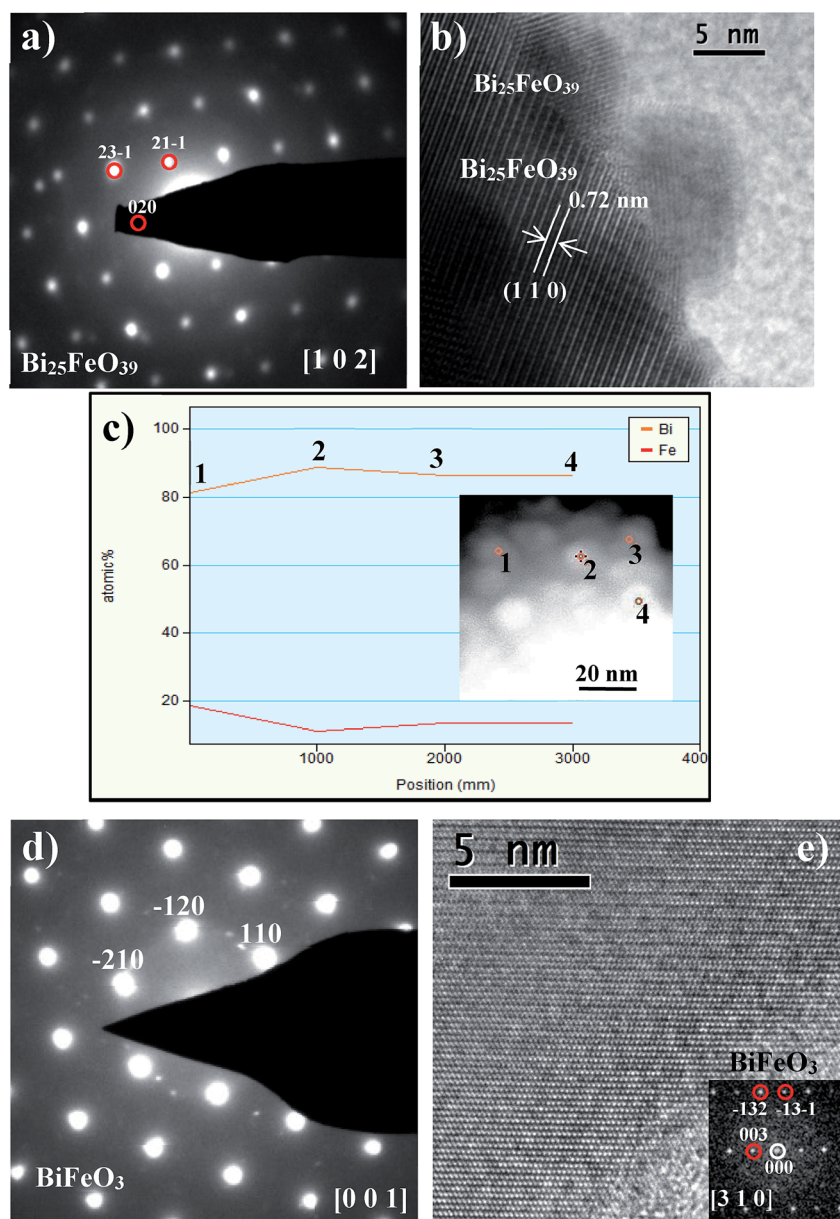
Fig. 10 (a) ED pattern of a $Bi_{25}FeO_{39}$ crystal along the [1 0 2] zone axis. (b) HRTEM image of some $Bi_{25}FeO_{39}$ crystals. (c) Four position profile EDS/HAADF analysis and the STEM image showing the positions where the EXD analysis was done. (d) ED pattern of a $BiFeO_3$ crystal along the [0 0 1] zone axis. (e) HRTEM micrograph of a $BiFeO_3$ crystal and the corresponding FFT in the inset along [3 1 0].

seconds. It is remarkable that the complex phases shown just before the flash for point #2 immediately react to produce single-phase $BiFeO_3$ as seen in Fig. 8b in such a short period of time. The chemical mappings, shown in Fig. 9, show a dense ceramic material with homogeneous distribution of iron and bismuth. TEM images of the specimen from point #3 confirm that the sample is monophasic $BiFeO_3$ with a rhombohedral structure ($R3c$ space group). Fig. 10d shows a dot-ED pattern oriented along the [0 0 1] zone axis of the rhombohedral $BiFeO_3$ structure, while Fig. 10e presents a HRTEM micrograph oriented along [3 1 0] with its FFT depicted in the inset. It is also of note that there is no evidence of an amorphous phase at grain boundaries leading to the inference that the reaction sintering occurred by solid-state mass transport mechanisms.

It is to be emphasized that reaction and consolidation take place simultaneously during the flash experiment. In conventional processing with bismuth and iron oxides the evolution of a secondary phase such as $Bi_2Fe_4O_9$ blocks the diffusion of Bi^{3+} ions into the Fe_2O_3 particles, making it difficult to obtain pure $BiFeO_3$.[48] It may be that the electric field amplifies the diffusion of Bi^{3+} into the Fe_2O_3 particles, which prevents the formation of the iron-rich secondary phase $Bi_2Fe_4O_9$, and therefore the reaction proceeds to the formation of phase-pure $BiFeO_3$.

The present results are different from those of experiments with the titania-alumina system during flash sintering, where sintering during the flash was followed by a reaction between alumina and titania when the specimen was held under current control for over 100 s.[58] In the present instance, the reaction occurs in just about 2 s and happens concurrently with sintering, just after the power peak. Clearly, the reaction pathway between these two sets of experiments is quite different, presumably reflecting the different chemistries.

In a recent work, flash experiments with three-phase ceramic composites constituted from equal volume fractions of α-Al_2O_3, $MgAl_2O_4$ spinel, and 8YSZ reported dissolution of alumina into the spinel phase to form a high-alumina spinel solid solution within 30 s at temperatures several hundreds of degrees below those required in conventional heating.[69] In the present case, the flash conditions also seem to enhance bismuth diffusion in $Bi_{25}FeO_{39}$ which forms just before the flash but then transforms into $BiFeO_3$ (by reacting with Fe_2O_3) in just a couple of seconds after the onset of the flash. The high homogeneity of the sample that is formed so rapidly under flash is quite remarkable. It may be related to recent discoveries by cathodoluminescence spectroscopy that show that the flash mechanism occurs within the grains rather than at the boundaries.[70]

5. Conclusions

Nanostructured and highly insulating, single-phase, $BiFeO_3$ specimens have been obtained by applying a small DC voltage to a mixture of Bi_2O_3 and Fe_2O_3 at a furnace temperature of 625 °C, in ambient air, in just a few seconds. The quality of the specimens depended on the applied field and the current limit set for the flash experiment; homogeneous and phase-pure specimens were obtained with a field of 50 V cm^{-1} and a current limit set to 35 mA mm^{-2}. The constituent oxides reacted and sintered simultaneously with the process being completed within seconds. Impedance spectroscopy measurements show the specimens to be homogeneous and highly insulating at room temperature.

The reaction mechanism was studied by *ex situ* X-ray diffraction measurements, high resolution TEM, and SEM-EDX of specimens obtained by interrupting the experiment at temperatures just before and just after the flash. Before flash the iron and bismuth oxides react to produce bismuth rich $Bi_{25}FeO_{39}$ along with residual Fe_2O_3. However, these phases transform into clean single-phase $BiFeO_3$ in a matter of a few seconds after the onset of the flash. The reaction is accompanied by sintering. The *absence* of amorphous phases at grain boundaries in the flashed specimens suggests that the process occurred by solid state diffusion. The electric field and current apparently unblock the diffusion of bismuth in the secondary phase, which is known to impede the reaction in conventional processing.

The new flash reaction sintering method reported here can be a breakthrough in material processing since it can enable the synthesis of complex oxides, which is normally not possible, or very difficult, in conventional methods, especially when the oxides are constituted from low melting and volatile elements and when the time–temperature processing schedule can encounter undesirable intermediate phases.

Conflicts of interest

There are no conflicts to declare.

Acknowledgements

References

1 C. N. R. Rao, *Chemical Approaches to the Synthesis of Inorganic Materials*, Wiley, New Delhi, 1994.

2 P. Balaz, M. Achimovicova, M. Balaz, P. Billik, Z. Cherkezova-Zheleva, J. M. Criado, F. Delogu, E. Dutkova, E. Gaffet, F. J. Gotor, R. Kumar, I. Mitov, T. Rojac, M. Senna, A. Streletskii and K. Wieczorek-Ciurowa, *Chem. Soc. Rev.*, 2013, **42**, 7571–7637.

3 C. Suryanarayana, *Prog. Mater. Sci.*, 2001, **46**, 1–184.

4 P. Lidström, J. Tierney, B. Wathey and J. Westman, *Tetrahedron*, 2001, **57**, 9225–9283.

5 K. J. Rao, B. Vaidhyanathan, M. Ganguli and P. A. Ramakrishnan, *Chem. Mater.*, 1999, **11**, 882–895.

6 Y. Wang, J. G. Yu, W. Xiao and Q. Li, *J. Mater. Chem. A*, 2014, **2**, 3847–3855.

7 T. Q. Chen, L. K. Pan, T. Lu, C. L. Fu, D. H. C. Chua and Z. Sun, *J. Mater. Chem. A*, 2014, **2**, 1263–1267.

8 S. C. Singh, H. B. Zeng, C. Guo and W. Cai, *Nanomaterials: Processing and Characterization with Lasers*, Wiley-VCH Verlag & Co. KGaA, Weinheim, 2012.

9 D. W. Liang, S. L. Wu, J. Liu, Z. F. Tian and C. H. Liang, *J. Mater. Chem. A*, 2016, **4**, 10609–10617.

10 J. C. Colmenares, E. Kuna and P. Lisowski, *Top. Curr. Chem.*, 2016, **374**, 59.

11 Z. A. Munir, U. Anselmi-Tamburini and M. Ohyanagi, *J. Mater. Sci.*, 2006, **41**, 763–777.

12 J. E. Garay, *Annu. Rev. Mater. Res.*, 2010, **40**, 445–468.

13 O. Guillon, J. Gonzalez-Julian, B. Dargatz, T. Kessel, G. Schierning, J. Räthel and M. Herrmann, *Adv. Eng. Mater.*, 2014, **16**, 830–849.

14 H. P. Ning, G. D. Mastrorillo, S. Grasso, B. L. Du, T. Mori, C. F. Hu, Y. Xu, K. Simpson, G. Maizza and M. J. Reece, *J. Mater. Chem. A*, 2015, **3**, 17426–17432.

15 A. Perejõn, N. Masõ, A. R. West, P. E. Sánchez-Jiménez, R. Poyato, J. M. Criado and L. A. Pérez-Maqueda, *J. Am. Ceram. Soc.*, 2013, **96**, 1220–1227.

16 R. Raj, *J. Eur. Ceram. Soc.*, 2012, **32**, 2293–2301.

17 K. Naik, S. K. Jha and R. Raj, *Scr. Mater.*, 2016, **118**, 1–4.

18 I. Bajpai, Y.-H. Han, J. Yun, J. Francis, S. Kim and R. Raj, *Adv. Appl. Ceram.*, 2016, **115**, 276–281.

19 V. M. Candelario, R. Moreno, R. I. Todd and A. L. Ortiz, *J. Eur. Ceram. Soc.*, 2017, **37**, 485–498.

20 M. Cologna, J. S. C. Francis and R. Raj, *J. Eur. Ceram. Soc.*, 2011, **31**, 2827–2837.

21 C. E. J. Dancer, *Mater. Res. Express*, 2016, **3**, 102001.

22 A. Gaur and V. M. Sglavo, *J. Mater. Sci.*, 2014, **49**, 6321–6332.

23 S. Grasso, E. Y. Kim, T. Saunders, M. Yu, A. Tudball, S. H. Choi and M. Reece, *Cryst. Growth Des.*, 2016, **16**, 2317–2321.

24 L. M. Jesus, R. S. Silva, R. Raj and J.-C. M'Peko, *J. Alloys Compd.*, 2016, **682**, 753–758.

25 S. K. Jha and R. Raj, *J. Am. Ceram. Soc.*, 2014, **97**, 527–534.

26 R. McKinnon, S. Grasso, A. Tudball and M. J. Reece, *J. Eur. Ceram. Soc.*, 2017, **37**, 2787–2794.

27 J.-C. M'Peko, J. S. C. Francis and R. Raj, *J. Eur. Ceram. Soc.*, 2014, **34**, 3655–3660.

28 A. L. G. Prette, M. Cologna, V. Sglavo and R. Raj, *J. Power Sources*, 2011, **196**, 2061–2065.

29 T. Saunders, S. Grasso and M. J. Reece, *Sci. Rep.*, 2016, **6**, 27222.

30 E. Zapata-Solvas, S. Bonilla, P. R. Wilshaw and R. I. Todd, *J. Eur. Ceram. Soc.*, 2013, **33**, 2811–2816.

31 Y. Zhang and J. Luo, *Scr. Mater.*, 2015, **106**, 26–29.

32 A. Roy, R. Gupta and A. Garg, *Adv. Condens. Matter Phys.*, 2012, 926290.

33 G. Catalan and J. F. Scott, *Adv. Mater.*, 2009, **21**, 2463–2485.

34 T. Gao, Z. Chen, Q. L. Huang, F. Niu, X. N. Huang, L. S. Qin and Y. X. Huang, *Rev. Adv. Mater. Sci.*, 2015, **40**, 97–109.

35 M. Bibes and A. Barthélémy, *Nat. Mater.*, 2008, **7**, 425–426.

36 Z. X. Li, Y. Shen, C. Yang, Y. C. Lei, Y. H. Guan, Y. H. Lin, D. B. Liu and W. Nan, *J. Mater. Chem. A*, 2013, **1**, 823–829.

37 I. Papadas, J. A. Christodoulides, G. Kioseoglou and G. S. Armatas, *J. Mater. Chem. A*, 2015, **3**, 1587–1593.

38 Z. Fan, K. Sun and J. Wang, *J. Mater. Chem. A*, 2015, **3**, 18809–18828.

39 H. Han, J. H. Lee and H. M. Jang, *Inorg. Chem.*, 2017, **56**, 11911–11916.

40 L. A. Perez-Maqueda, E. Gil-Gonzalez, A. Perejon, J. M. Lebrun, P. E. Sanchez-Jimenez and R. Raj, *J. Am. Ceram. Soc.*, 2017, **100**, 3365–3369.

41 J. Rodriguez-Carvajal, *Presented in Part at the Satellite Meeting on Powder Diffraction of the XV Congress of the IUCr*, 1990.

42 Y. Dong, I. W. Chen and L. Gaukler, *J. Am. Ceram. Soc.*, 2015, **98**, 2333–2335.

43 J. T. S. Irvine, D. C. Sinclair and A. R. West, *Adv. Mater.*, 1990, **2**, 132–138.

44 A. Perejon, N. Murafa, P. E. Sanchez-Jimenez, J. M. Criado, J. Subrt, M. J. Dianez and L. A. Perez-Maqueda, *J. Mater. Chem. C*, 2013, **1**, 3551–3562.

45 A. Perejon, P. E. Sanchez-Jimenez, J. M. Criado and L. A. Perez-Maqueda, *J. Phys. Chem. C*, 2014, **118**, 26387–26395.

46 R. Haumont, I. A. Kornev, S. Lisenkov, L. Bellaiche, J. Kreisel and B. Dkhil, *Phys. Rev. B: Condens. Matter Mater. Phys.*, 2008, **78**, 134108.

47 S. M. Selbach, M.-A. Einarsrud and T. Grande, *Chem. Mater.*, 2009, **21**, 169–173.

48 M. S. Bernardo, T. Jardiel, M. Peiteado, A. C. Caballero and M. Villegas, *J. Eur. Ceram. Soc.*, 2011, **31**, 3047–3053.

49 F. Gheorghiu, M. Calugaru, A. Ianculescu, V. Musteata and L. Mitoseriu, *Solid State Sci.*, 2013, **23**, 79–87.

50 A. R. Makhdoom, M. J. Akhtar, R. T. A. Khan, M. A. Rafiq, M. M. Hasan, F. Sher and A. N. Fitch, *Mater. Chem. Phys.*, 2013, **143**, 256–262.

51 T. T. Carvalho and P. B. Tavares, *Mater. Lett.*, 2008, **62**, 3984–3986.

52 A. Maître, M. François and J. C. Gachon, *J. Phase Equilib. Diffus.*, 2004, **25**, 59–67.

53 M. Muneeswaran, R. Dhanalakshmi and N. V. Giridharan, *Ceram. Int.*, 2015, **41**, 8511–8519.

54 Y. P. Wang, L. Zhou, M. F. Zhang, X. Y. Chen, J. M. Liu and Z. G. Liu, *Appl. Phys. Lett.*, 2004, **84**, 1731–1733.

55 S. R. Das, R. N. P. Choudhary, P. Bhattacharya, R. S. Katiyar, P. Dutta, A. Manivannan and M. S. Seehra, *J. Appl. Phys.*, 2007, **101**, 034104.

56 G. L. Yuan, S. W. Or, Y. P. Wang, Z. G. Liu and J. M. Liu, *Solid State Commun.*, 2006, **138**, 76–81.

57 K. Terauds, J.-M. Lebrun, H.-H. Lee, T.-Y. Jeon, S.-H. Lee, J. H. Je and R. Raj, *J. Eur. Ceram. Soc.*, 2015, **35**, 3195–3199.

58 S. K. Jha, J. M. Lebrun and R. Raj, *J. Eur. Ceram. Soc.*, 2016, **36**, 733–739.

59 W. Ji, B. Parker, S. Falco, J. Y. Zhang, Z. Y. Fu and R. I. Todd, *J. Eur. Ceram. Soc.*, 2017, **37**, 2547–2551.

60 R. Raj and H. Chan, *J. Am. Ceram. Soc.*, 2016, **99**, 3226–3232.

61 J. M. Lebrun, C. S. Hellberg, S. K. Jha, W. M. Kriven, A. Steveson, K. C. Seymour, N. Bernstein, S. C. Erwin and R. Raj, *J. Am. Ceram. Soc.*, 2017, **100**, 4965–4970.

This journal is © The Royal Society of Chemistry 2018

J. Mater. Chem. A, 2018, **6**, 5356–5366 | 5365

62 J. M. Lebrun, T. G. Morrissey, J. S. C. Francis, K. C. Seymour, W. M. Kriven and R. Raj, *J. Am. Ceram. Soc.*, 2015, **98**, 1493–1497.

63 H. Majidi and K. van Benthem, *Phys. Rev. Lett.*, 2015, **114**, 195503.

64 J. F. Rufner, D. Kaseman, R. H. R. Castro, K. van Benthem and G. Rohrer, *J. Am. Ceram. Soc.*, 2016, **99**, 1951–1959.

65 C. Korte, N. D. Zakharov and D. Hesse, *Phys. Chem. Chem. Phys.*, 2003, **5**, 5530–5535.

66 T. Kondo, M. Yasuhara, T. Kuramoto, Y. Kodera, M. Ohyanagi and Z. A. Munir, *J. Mater. Sci.*, 2008, **43**, 6400–6405.

67 K. J. D. Mackenzie, R. K. Banerjee and M. R. Kasaai, *J. Mater. Sci.*, 1979, **14**, 333–338.

68 D. Cai, J. Li, T. Tong, D. Jin, S. Yu and J. Cheng, *Mater. Chem. Phys.*, 2012, **134**, 139–144.

69 D. Kok, S. K. Jha, R. Raj and M. L. Mecartney, *J. Am. Ceram. Soc.*, 2017, **100**, 3262–3268.

70 H. Gao, T. J. Asel, J. W. Cox, Y. Zhang, J. Luo and L. J. Brillson, *J. Appl. Phys.*, 2016, **120**, 105302.